NASA TECHNICAL PAPER

SECONDARY FLOW SPANWISE DEVIATION MODEL FOR THE STATORS OF NASA MIDDLE COMPRESSOR STAGES

WILLIAM B. ROBERTS

AND

DONALD M. SANDERCOCK

Lewis Research Center
Cleveland, Ohio

February, 1984

GRANT NAG 3-212

SCHOOL OF ENGINEERING
UNIVERSITY OF SANTA CLARA
SANTA CLARA, CA 95053

NASA TECHNICAL PAPER

SECONDARY FLOW SPANWISE DEVIATION MODEL FOR THE STATORS OF NASA MIDDLE COMPRESSOR STAGES

WILLIAM B. ROBERTS

AND

DONALD M. SANDERCOCK

Lewis Research Center
Cleveland, Ohio

February, 1984

GRANT NAG 3-212

SCHOOL OF ENGINEERING
UNIVERSITY OF SANTA CLARA
SANTA CLARA, CA 95053

SUMMARY

A model of the spanwise variation of deviation for stator blades is presented. Deviation is defined as the difference between the passage mean flow angle and the metal angle at the outlet of a blade element of an axial compressor stage. The variation of deviation is taken as the difference above or below that predicted by blade element, i.e., two-dimensional, theory at any spanwise location.

The variation of deviation is dependent upon the blade camber, solidity and inlet boundary layer thickness at the hub or tip end-wall, and the blade channel aspect ratio. If these parameters are known or can be calculated, the model provides a reasonable approximation of the spanwise variation of deviation for most compressor middle stage stators operating at subsonic inlet Mach numbers.

INTRODUCTION

The development of a spanwise deviation model for stators was done before the rotor model because the effects of rotation and end-wall gap could be ignored. These factors lead to a significantly different variation of deviation between rotors and stators, as will be shown.

A model for the spanwise distribution of deviation can be split into two parts: the prediction of (1) primary or two-dimensional blade element deviation, and (2) secondary flow or end-wall induced deviation. This paper considers alternative (2).

NASA data [1]* from twelve (12) subsonic, middle stage rotor/stator combinations have been considered to form a model of stator spanwise secondary flow induced deviation. All data considered was from operation at the design tip speed of 244 meters per second and maximum efficiency. A summary plot of this data is shown in Figure 1. There, the measured deviation, δ†, minus a calculated two-dimensional equivalent deviation, δ_{eq}, [2] is plotted versus percent span. If the equivalent deviation was correct and the flow near mid-span was approximately axi-symmetrical (i.e., two-dimensional in the blade element plane), the mid-span values of $\delta - \delta_{eq}$ shown on Figure 1 would be zero. That it is not implies a lack of core flow, an error in the calculated blade element performance, or both. If it is assumed that the calculated blade element deviation is mainly at fault, then a replot of the data on Figure 1 with the mid-span value of $\delta - \delta_{eq}$ set at zero would give the spanwise variation of deviation due to secondary flow, i.e.,

$\bar{\Delta} = \Delta\delta - (\Delta\delta)_{50} = (\delta - \delta_{eq}) - (\delta - \delta_{eq})_{50}$, where $(\delta - \delta_{eq})_{50}$

---

*Numbers in brackets denote references at the end of the report.
†Symbol definition in Appendix A.

is the midspan value. This has been done; the results for each stator combined with various rotors are given in Appendix B.

Figure 2 shows the difference between rotor and stator spanwise variation of deviation. There the spanwise variation due to secondary flow is plotted for rotor 23B/stator 20 operating together [1] using the method described above. It can be seen that the rotor has overturning at the hub and underturning at the tip with little variation between. This is probably due to the effect of rotation on the fluid in the blade wake. This fluid is centrifuged to the tip region. The gap at the tip would further increase the underturning due to the accumulation of low energy fluid at the tip.

For stators with no end-wall gaps, there are two distinct maximums of underturning that occurs near the end-walls as seen in Figure 2. These maximums are caused by the "rolling up" of the two major secondary, viscous corner vortices that form because of the passage pressure gradient. The wall side of the vortex enhances overturning and the mid-passage side underturning due to the direction of rotation, see Figure 3.

The physical parameters that can affect stator spanwise distribution of deviation are blade camber, $\emptyset$, blade aspect ratio, AR, blade channel aspect ratio , AR_c, solidity, σ, end-wall boundary layer thickness at the inlet, represented by

the inlet boundary layer displacement thickness, δ_1^*, and perhaps hub/tip radius ratio. All of the above parameters are available for all the rotor/stator combinations except displacement thickness. However, Reference 3 gives values of δ_1^* for seven (7) of the rotor/stator pairs. A list of these combinations, along with pertinent physical parameters, is given in Table 1.

A perusal of the data plots in Appendix B shows that, for most stators, there is a maximum underturning that occurs within 10-20% of the end-walls with an unsymmetrical exponential type variation between there and the end-wall or mid-span. Therefore, the variation of secondary flow induced deviation has been modeled in four (4) parts: (1) the magnitude of the maximum underturning, (2) the location of the maximum underturning, (3) the value of underturning or overturning at the end-wall and (4) the variation between. A schematic of this model is shown in Figure 4.

THE MAGNITUDE OF MAXIMUM UNDERTURNING

A series of physical models for maximum underturning that reflect various combinations of the parameters listed in Table 1 is given in Table 2. The criterion adopted for an acceptable

model is the ability to correlate $\bar{\Delta}_{max}$ within $\pm 1^{o}$. This value was chosen because that is the expected accuracy of the data [1]. Example plots of data from Table 1 using some of these models are given in Reference 4. Hub/tip radius ratio was not included in these models because it was constant at 0.8.

Model 1 was an attempt to account for the maximum underturning using commonly-available geometrical parameters. The plot of Model 1 versus $\bar{\Delta}_{max}$ indicates that something essential has been left out, see Figure 5. A perusal of the literature on secondary flow [5, 6] indicates that the end-wall boundary layers have a significant effect on secondary loss and turning in cascades and rotors. This is natural, since secondary flow is the redistribution of the end-wall boundary layer as it passes through the blade row. The stators of Table 1 are those for which the boundary layer properties were available at the tip. Inlet displacement thickness was chosen as the parameter to represent the boundary layer effect. Figure 6 shows the variation of $\bar{\Delta}_{max}$ with δ_1^*. As can be seen, the correlation is significant.

The remainder of the models tested had displacement thickness in the numerator. For the thirteen remaining models, only 5 and 7 correlated all the data within $\pm 1^{o}$. Of these two, Model 5 has the best fit with the data. Figure 7 shows the linearized version of Model 5. From this, the relation between

the maximum value of underturning and the important physical parameters can be deduced:

$$\bar{\Delta}_{max} = 150 \left[\frac{\phi (\delta_1^*)^2}{AR_c \cdot \sigma} \right]^{3/4} \quad \text{(deg)} \qquad (1)$$

Equation 1 is a specific relationship modeling NASA middle stage data [1]. However, the model should be applicable to similar subsonic compressor stages. Therefore, it would be useful to have Equation 1 in a general form. This can be done by appropriately normalizing the parameters in the bracket. The terms in the denominator are already dimensionless, so the camber and displacement thickness are the parameters that should be modified. The camber can be non-dimensionalized by specifying its value in radians. It is physically logical to normalize the displacement thickness by the mean blade height. If an inlet boundary layer is large compared to the blade height, the effect on spanwise deviation should be large and vice versa. A drawback in this case is that the data used to make up the model all had the same blade height of 10.16 cm and there is no acceptable data available with a different height. Therefore, the general model will be unproven for different blade heights.

The non-dimensional linear model for maximum underturning is given below and in Figure 8 with the constant of proportionality adjusted to reflect camber, ϕ, in radians and inlet displacement thickness normalized by blade height or span, δ_1^*/s:

$$\bar{\Delta}_{max} = 2.5 \times 10^4 \left[\frac{\phi(\delta_1^*/s)^2}{AR_c \cdot \sigma} \right]^{3/4} \quad \text{(deg)} \qquad (2)$$

LOCATION OF MAXIMUM UNDERTURNING

Table 3 lists the location of maximum underturning for twelve (12) NASA rotor/stator combinations and the exit of Stator 3 of the General Electric Low-Speed Research Compressor [7]. A plot of this data, shown in Figure 9, shows that the maximum underturning location clusters between ten to twenty percent of span ($\bar{s}_m$ = 0.1-0.2) from the hub or tip. A careful study of the data indicates that there is no combination of parameters that model this result. All the NASA data is from test stages with a hub/tip radius ratio of 0.8, so this could be a correlating factor, although the GE stator has a radius ratio of 0.7 and it clusters with the NASA data. When the final model was compared to the data it was found that the best fit occurred when the location of maximum underturning $\bar{\Delta}_{max}$, was taken as 12.5 percent of the blade span (i.e., height) from the end-wall.

This agrees well with the average of the locations shown in Figure 9. Therefore, until additional data is available, the location of maximum underturning will be taken between ten and twenty percent of span from the hub or tip with an arbitrary value of twelve and one half percent, i.e.:

$$\bar{s}_{m-h} = \bar{s}_{m-t} = 0.125 \qquad (3)$$

END WALL VALUES

To completely model the spanwise variation of deviation, the value of under or overturning, $\bar{\Delta}_w$, must be estimated at the wall. This can be done by extrapolating the data of Appendix B. The method used was to fit a curve through the 15%, 10% and 5% span data points and on to the wall. This is illustrated in Figure 10, where it can be seen that there is a region of "reasonable" maximum to minimum extrapolation.

Since the value of deviation difference at the wall is the result of the same corner vortex that causes maximum underturning, and the strength of this vortex will be proportional to the difference between $\bar{\Delta}_{max}$ and the value at the wall, the same parameters that modeled $\bar{\Delta}_{max}$ should model the difference:

$$(\bar{\Delta}_{max} - \bar{\Delta}_w) \sim \frac{\phi(\delta_1^*/s)^2}{AR_c \cdot \sigma}$$

Table 4 shows the appropriate parameters, with values of $\bar{\Delta}_w$ adjusted within the region of maximum to minimum extrapolation to best fit the model. Figure 11 shows that with the exception of one data point there is a linear relation between deviation difference and the vortex parameter:

$$\bar{\Delta}_{max} - \bar{\Delta}_w = 5.7 \times 10^5 \left[\frac{\phi(\delta_1^*/s)^2}{AR_c \cdot \sigma}\right] \quad \text{(deg)} \qquad (4)$$

Once $\bar{\Delta}_{max}$ is known, $\bar{\Delta}_w$ can be calculated using Equation 4.

SPANWISE VARIATION

After the values of the maximum and wall deviation difference and the location of the former have been found, the variation between the mid-span and the wall must be determined. The variations plotted in Appendix A indicate that a modified normal distribution could be used. After a data fitting process

the following relations have been adopted:

1) The variation between the location of maximum underturning to the mid-span (where $\bar{\Delta} = 0$) is modeled by:

$$\bar{\Delta} = \bar{\Delta}_{max} \left[e^{-(6x/s)^2} \right] \quad \text{(deg)} \tag{5}$$

where x is the spanwise distance from the location of $\bar{\Delta}_{max}$ to the mid-span and s is the mean blade span or height, $0 \leq \frac{x}{s} \leq 0.375$.

2) The variation between the location of maximum underturning to the wall is modeled by:

$$\bar{\Delta} = \bar{\Delta}_{max} - (\bar{\Delta}_{max} - \bar{\Delta}_{w}) \left[e^{-(20\ x/s)^2} \right] \text{(deg)} \tag{6}$$

where x is the spanwise distance from the location of $\bar{\Delta}_{max}$ to the wall and s is the mean blade span or height, $0 \leq \frac{x}{s} \leq 0.125$.

Equations 5 and 6 apply in both the hub or tip region.

RESULTS AND DISCUSSION

The model, Equations 2 through 6, has been compared with experimental half-span tip region distributions for the stators of Table 1 (using Appendix B). The results are shown in Figure 12. There it can be seen that the prediction is fair to good for all stators with the exc ,cion of stator 22 (Fig. 12f). Therefore, the present model can be considered to be a good approximation for subsonic NASA middle stages of medium hub/tip radius ratio.

Before the model is applied outside the range of the data base [1], it should be validated against appropriate data, i.e., that which includes the inlet boundary layer displacement thickness. Unfortunately, additional data of this type is not currently available to the authors. Until such data is available, the model should be treated as preliminary. However, there is one factor that has been demonstrated: the effect of the end-wall boundary layer on the spanwise variation of deviation. It has been long known that the end-wall boundary layer is a primary factor in the development of secondary flows. However, most attempts to model the loss and deviation variation caused by end-wall effects have ignored the specification, estimation, or calculation of end-wall boundary layer thickness variation through the compressor. This can no longer be

neglected. Furthermore, future research compressor data should specify hub and tip boundary layer development for at least design point operation. Such data would be of great benefit to the model analysts and computational fluid dynamicists.

CONCLUSION

It has been demonstrated that the following five (5) equation models can predict the spanwise variation of deviation to a good approximation for NASA subsonic middle stages (applies for the hub and tip regions):

Value of maximum underturning,

$$\bar{\Delta}_{max} = 2.5 \times 10^4 \left[\frac{Q(\delta_1^*/s)^2}{AR_c \cdot \sigma} \right]^{3/4} \quad \text{(deg)}$$

Location of maximum underturning, $(\bar{s})_{max} = 0.125$

Value at the wall, $\bar{\Delta}_w = \bar{\Delta}_{max} - 5.7 \times 10^5 \left[\frac{Q(\delta_1^*/s)^2}{AR_c \cdot \sigma} \right]$ (deg)

Variation from location of maximum underturning to midspan,

$$\bar{\Delta} = \bar{\Delta}_{max} \left[e^{-(6x/s)^2} \right] \quad \text{(deg)}$$

Variation from location of maximum underturning to the wall,

$$\bar{\Delta} = \bar{\Delta}_{max} - \left(\bar{\Delta}_{max} - \bar{\Delta}_{w} \right) \left[e^{-(20\ x/s)^2} \right] \quad \text{(deg)}$$

This model has not been tested outside the data base. However, it should prove useful for making engineering predictions of spanwise variation of deviation for stators if (1) the distribution of two-dimensional blade element deviation is available, (2) there is a region of axi-symmetric core flow and (3) the inlet Mach number is less than one.

REFERENCES

1. Britsch, W. R., et al: Effects of Diffusion Factor, Aspect Ratio, and Solidity on Overall Performance of 14 Compressor Middle Stages. NASA Technical Paper 1523, September 1979.

2. Unpublished notes of D. M. Sandercock, NASA-Lewis Research Center, 1982.

3. Roberts, W. B., et al: Boundary Layer Development Through the Tip Regions of Core Compressor Stages. Final Scientific Report, NASA Grant NAS 3133, August 1978.

4. Roberts, W. B.: Secondary Flow Spanwise Deviation Model for NASA Core Stators. Progress Report on NASA Grant NAG 3-212, March 1983.

5. Salvage, J. W.: A Review of the Current Concept of Cascade Secondary Flow Effects. VKI Tech. Note 95, March 1974.

6. Adkins, G.G., Jr. and Smith, L. H., Jr.: Spanwise Mixing in Axial-Flow Turbomachines. ASME Paper No. 81-GT-57. March 1981.

7. Smith, L. H., Jr.: Casing Boundary Layers in Multistage Axial-Flow Compressors, in Flow Research on Blading, L. S. Dzung, ed., Elsevier, Amsteram, 1970, p. 275.

APPENDIX A

SYMBOLS

AR	-	aspect ratio
AR_c	-	channel aspect ratio
s	-	span or blade height
$\bar{s}_m$	-	fraction of the span to the location of maximum underturning from hub or tip
x	-	distance along the span
δ	-	deviation angle
$\bar{\Delta}$	-	difference in deviation, $(\delta - \delta_{eq}) - (\delta - \delta_{eq})_{50}$
δ^*	-	boundary layer displacement thickness
σ	-	blade solidity
θ	-	blade camber

Subscripts

1	-	inlet
50	-	mid-span
eq	-	equivalent
h	-	hub
max	-	maximum
t	-	tip
w	-	end-wall

APPENDIX B

Variation of Deviation Due to Secondary Flow for NASA Middle Stage Stators Combined with Various Rotors

ORIGINAL PAGE IS
OF POOR QUALITY

K&E 10 X 10 TO THE ½ INCH 359-11
KEUFFEL & ESSER CO. MADE IN U.S.A.

TABLE 1. NASA CORE STATORS

Secondary Flow Geometry and Performance

Stator	AR_c	AR	ϕ_t (deg)	ϕ_h (deg)	σ_t	σ_h	$\bar{s}_{m,t}$	$\bar{\Delta}_{max,t}$ (deg)	$\bar{s}_{m,h}$	$\bar{\Delta}_{max,h}$ (deg)	$\delta^*_{t_1}$ (in.)	Symbol
20 (Rotor 23B)	1.90	1.04	55.4	60.5	1.60	2.00	0.100	4.1	0.15	1.5	.020	○
20 (Rotor 24A)							0.150	6.5	0.10	3.7	.027	△
20B (Rotor 25A)	1.42				1.20	1.50	0.100	5.6	0.20	2.0	.022	□
20C (Rotor 23D)	2.34				2.00	2.50	0.125	2.4	0.30	0.8	.018	◇
20C (Rotor 24B)							0.100	4.6	0.10	2.3	.032	⊿
21 (Rotor 27C)	2.48	1.24	68.5	72.4	1.80	2.25	0.150	6.0	0.15	6.0	.027	▱
22 (Rotor 28D)	1.63	0.82	82.5	83.9	1.80	2.25	0.230	1.2	0.15	2.0	.010	⌂

TABLE 2. MODELS FOR MAXIMUM UNDERTURNING

Model No.	Model, $\bar{\Delta}_{max}$ =	Model No.	Model, $\bar{\Delta}_{max}$ =
1	$\frac{K\phi}{AR \cdot AR_c \sqrt{\sigma}}$	8	$\frac{K\phi(\delta_1^*)^2}{\sqrt{AR_c}\sigma}$
2	$\frac{K\phi\delta_1^*}{AR\sqrt{\sigma}}$	9	$\frac{K\phi(\delta_1^*)^2}{AR_c\sqrt{\sigma}}$
3	$\frac{K\phi\delta_1^*}{AR \cdot AR_c}$	10	$\frac{K\phi(\delta_1^*)^2}{AR_c}$
4	$\frac{K\phi\delta_1^*}{AR \cdot AR_c \cdot \sigma}$	11	$\frac{K\phi(\delta_1^*)^2}{\sigma}$
5	$\frac{K\phi(\delta_1^*)^2}{AR_c \cdot \sigma}$	12	$\frac{K\phi\ \delta_1^*}{AR_c}$
6	$\frac{K\phi(\delta_1^*)^2}{(AR_c \cdot \sigma)^{3/4}}$	13	$\frac{K(\delta_1^*)^2}{AR_c}$
7	$\frac{K\phi(\delta_1^*)^{2.5}}{AR_c \cdot \sigma}$	14	$\frac{K\ \delta_1^*}{(AR_c)^2}$

Nomenclature:

- AR - Blade Aspect Ratio
- AR_c - Channel Aspect Ratio
- K - Constant
- δ_1^* - End-Wall Displacement Thickness at Inlet
- ϕ - Blade Camber at hub or tip

TABLE 3.

SPANWISE POSITION OF MAXIMUM UNDERTURNING FOR NASA STATORS

Stator	$\bar{s}_{m,h}$ †	$\bar{s}_{m,t}$ †	$\delta^*_{i,t}$ (in.)	AR_c	AR	σ_t
20 (R23B)	.125	.100	.020	1.90	1.04	1.16
20 (R24A)	.100	.150	.027	1.90	1.04	1.6
20C (R23D)	.300	.150	.018	2.34	1.04	2.0
20C (R24B)	.150	.125	.032	2.34	1.04	2.0
20B (R25A)	.150	.100	.022	1.42	1.04	1.2
21 (R26B)	.150	.100	-	2.48	1.24	1.8
21 (R27A)	.150	.100	-	2.48	1.24	1.8
21 (R27C)	.100	.150	.027	2.48	1.24	1.8

Stator	$\bar{s}_h$	$\bar{s}_t$	$\delta^*_{i,t}$ (in.)	AR_c	AR	σ_t
21D (R26D)	.10	.15	-	1.24	1.24	0.9
21D (R27D)	.05	.15	-	1.24	1.24	0.9
22 (R28B)	.15	-	-	1.63	0.82	1.8
22 (R28D)	.15	.20	.01	1.63	0.82	1.8
LSRC No. 3 Stator	.20	.10	-			

Avg. $\bar{s}_{m,h}$ = .144

Avg. $\bar{s}_{m,t}$ = .121

†$\bar{s}_{m,h}$ - % span from hub, $\bar{s}_{m,t}$ - % span from tip.

TABLE 4. TIP END-WALL VALUES OF THE DIFFERENCE IN DEVIATION

Stator	$\bar{\Delta}_{max,t}$ (deg)	$\bar{\Delta}_{w,t}$ (deg)	$\bar{\Delta}_{max,t} - \bar{\Delta}_{w,t}$ (deg)	Symbol
20 (Rotor 23B)	4.1	0	4.1	○
20 (Rotor 24A)	6.5	-2.5	9.0	△
20B (Rotor 25A)	5.6	-3.0	8.6	□
20C (Rotor 23D)	2.4	0.5	1.9	◇
20C (Rotor 24B)	4.6	-2.0	6.6	▷
21 (Rotor 27C)	6.0	-1.5	7.5	⌂
22 (Rotor 28D)	1.2	-4.8	6.0	⬠

FIGURE 1.

SPANWISE DEVIATION PERFORMANCE OF NASA STATORS IN COMBINATION WITH VARIOUS ROTORS AT MAXIMUM EFFICIENCY OPERATION

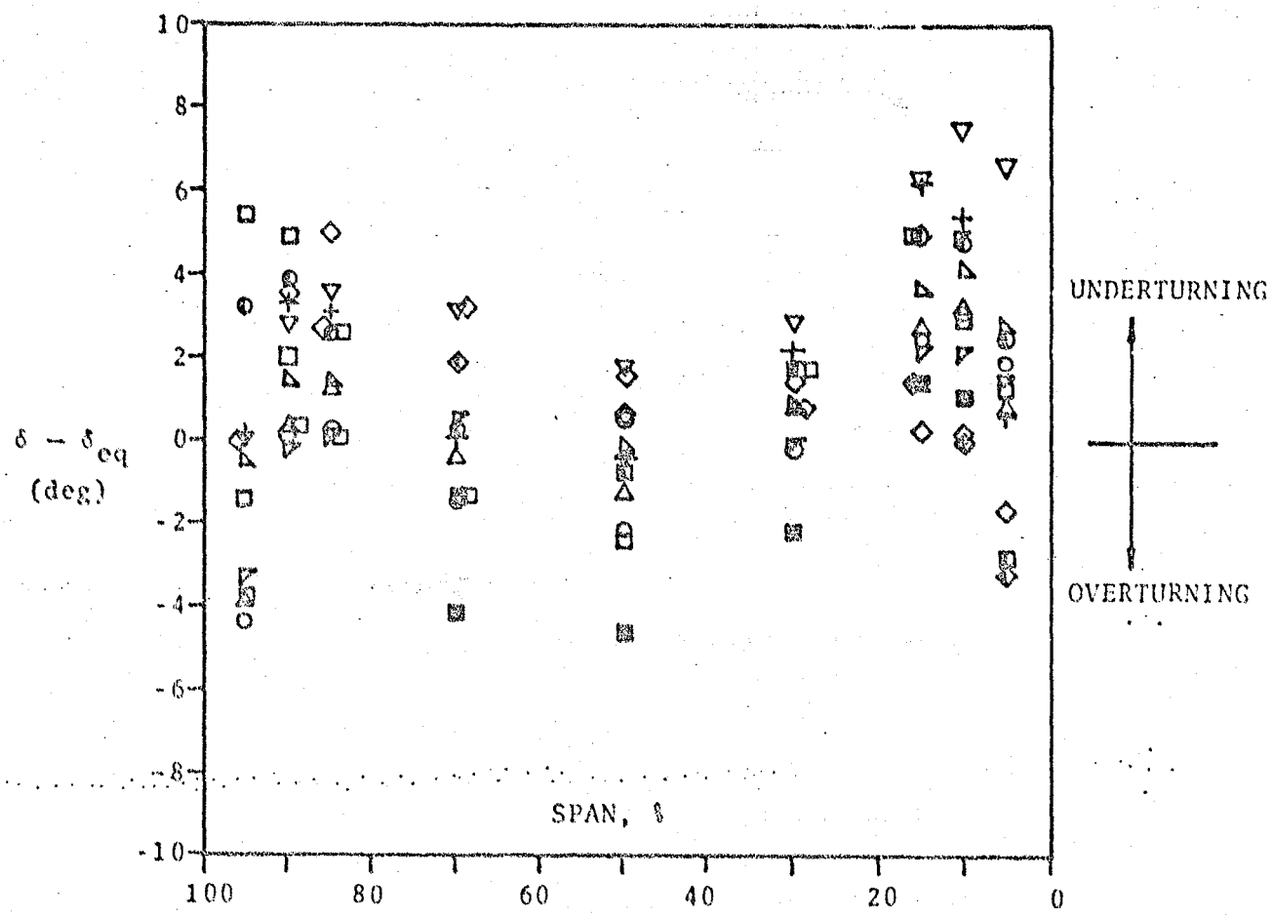

	ROTOR	STATOR		ROTOR	STATOR
△	23B	20	◐	26D	21D
+	24A		■	27D	
▽	23D	20C			
△	24B		◇	28B	22
▽	25A	20B			
○	26B		◈	28D	
□	27A	21			
▣	27C				

FIGURE 2. COMPARISON BETWEEN ROTOR AND STATOR SPANWISE VARIATION OF DEVIATION

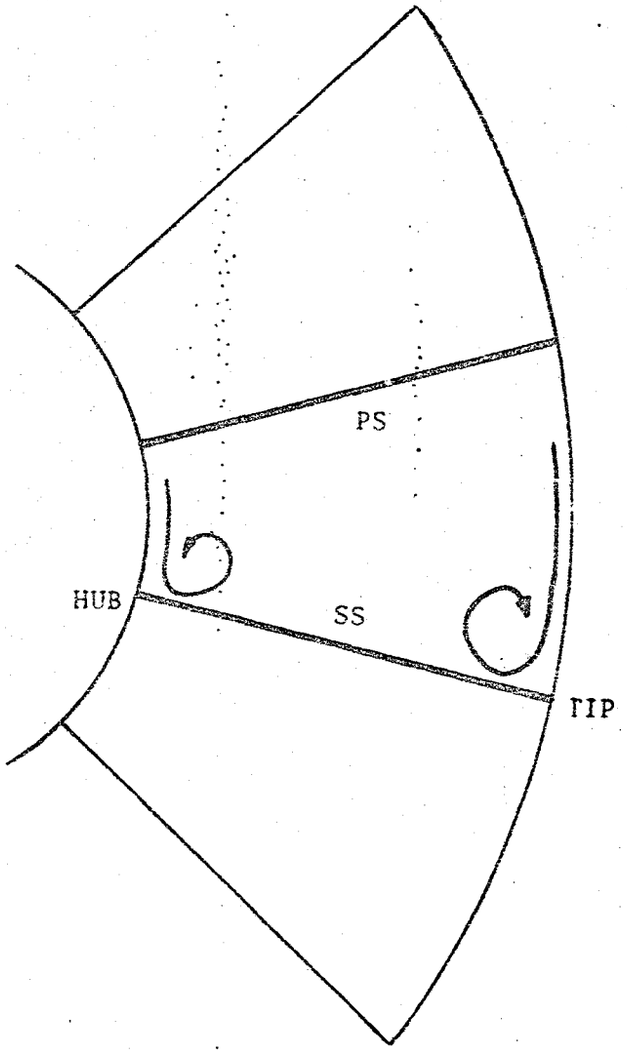

SS - SUCTION SURFACE

PS - PRESSURE SURFACE

FIGURE 3. SCHEMATIC OF VISCOUS END-WALL VORTICIES FOR STATORS

FIGURE 4.

MODEL FOR THE VARIATION OF
SECONDARY FLOW INDUCED DEVIATION

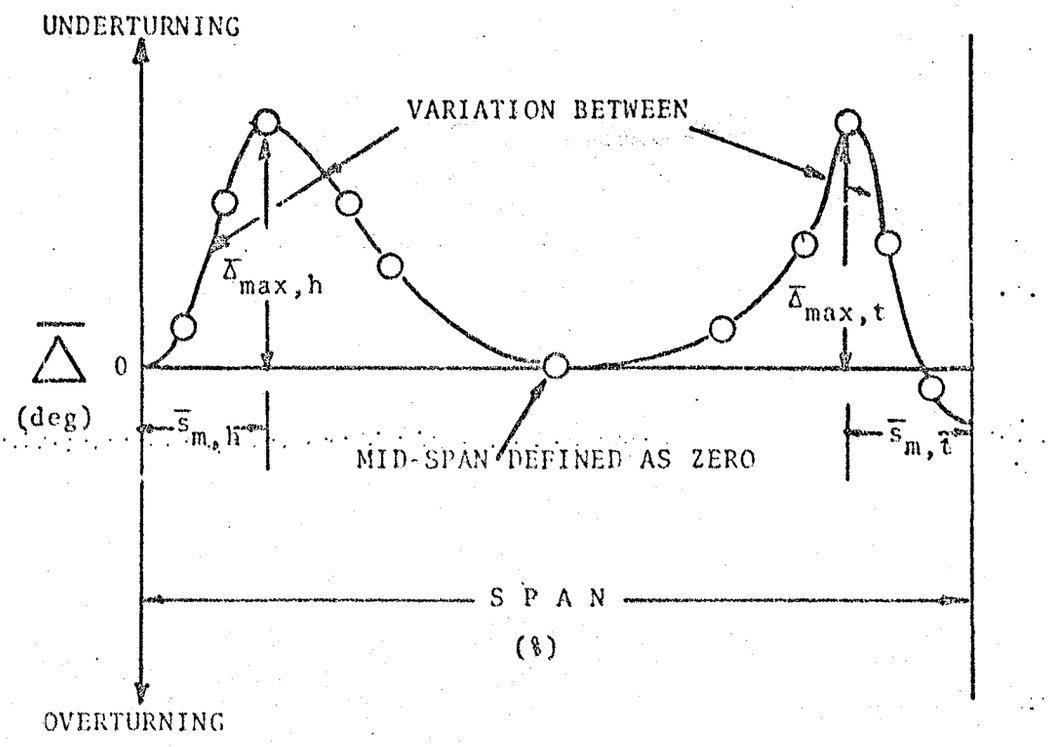

Nomenclature:

$\overline{\Delta}$	-	$\Delta\delta - (\Delta\delta)_{\delta_0}$, $\Delta\delta = \delta - \delta_{eq}$
$\overline{\Delta}_{max}$	-	Maximum Underturning
$\overline{s}_m$	-	$\left(\frac{x}{\overline{s}}\right)_m$ - Fraction of span to maximum underturning from hub or tip
h	-	hub
t	-	tip

FIGURE 5.

NASA STATORS

MODEL 1
(deg)

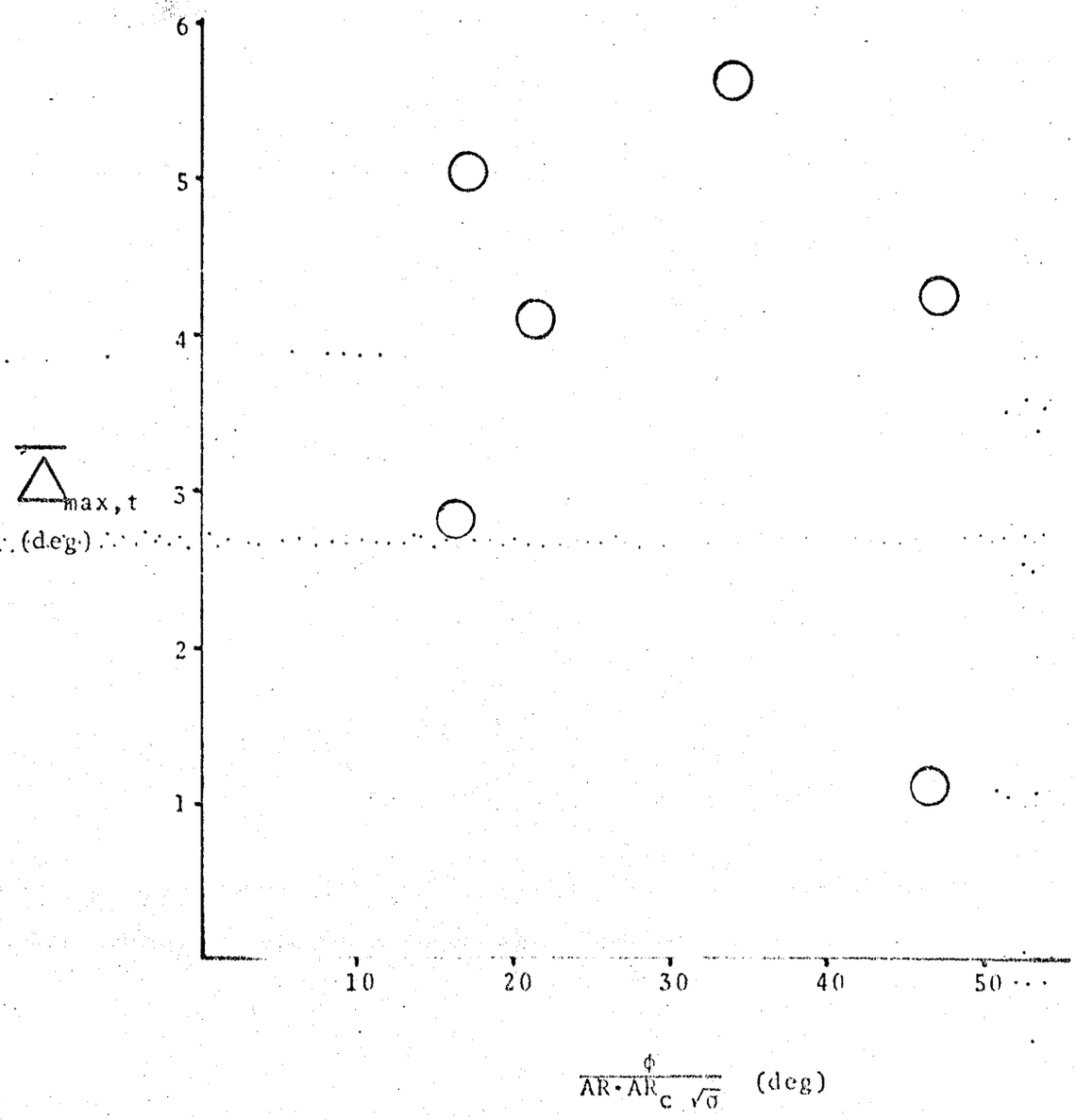

FIGURE 6.

MAXIMUM UNDERTURNING VERSUS
INLET TIP DISPLACEMENT THICKNESS
FOR NASA STATORS

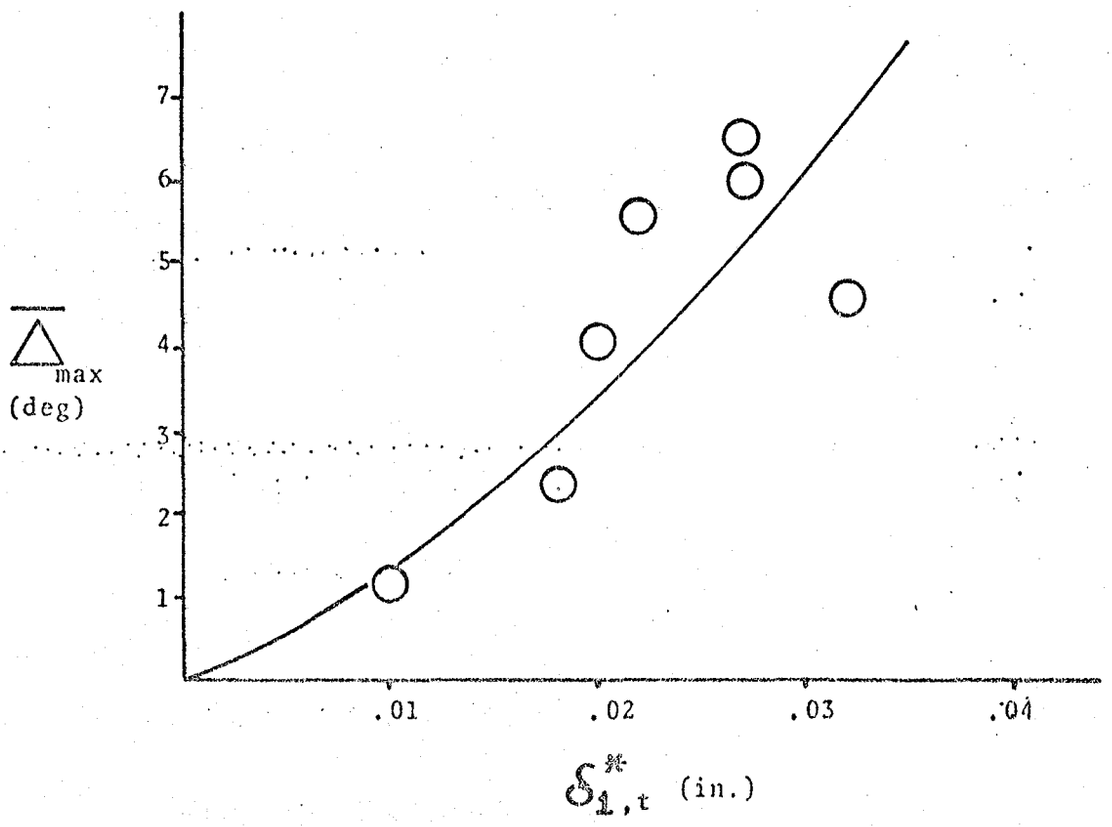

FIGURE 7.

CORRELATION OF MAXIMUM UNDERTURNING

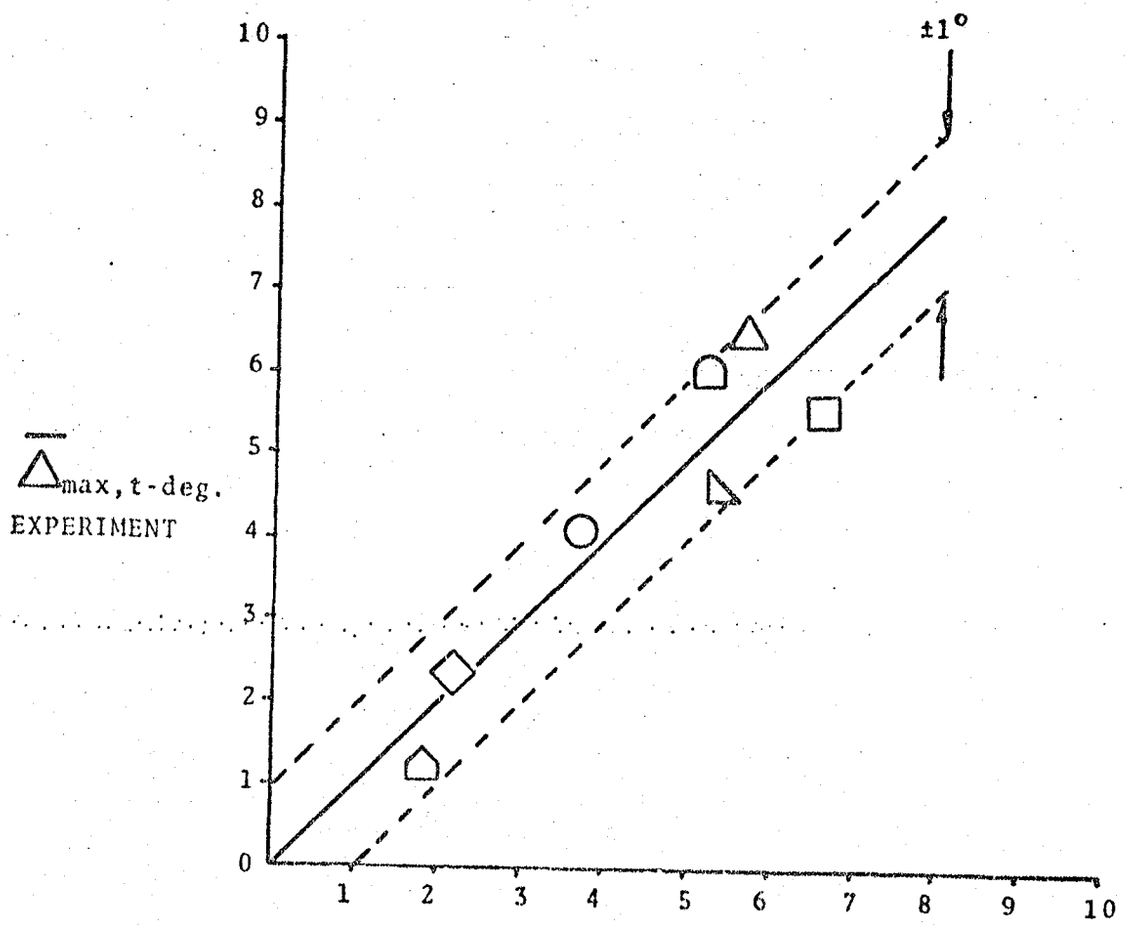

$$\overline{\Delta}_{max} = 150 \left[\frac{\phi(\delta_1^*)^2}{AR_c \cdot \sigma}\right]^{3/4}, \text{ deg.}$$

FIGURE 8.

CORRELATION OF MAXIMUM UNDERTURNING
USING NON-DIMENSIONAL MODEL

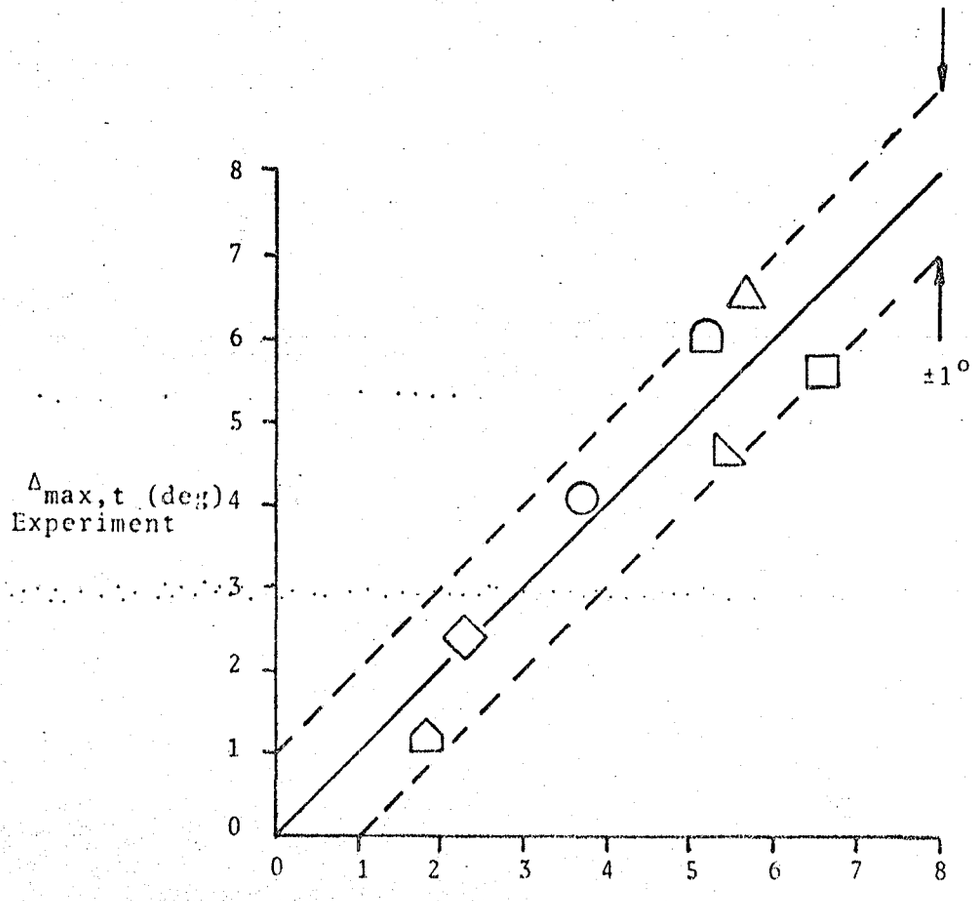

$$\bar{\Delta}_{max} = 2.5 \times 10^{4} \left[\frac{\phi (\delta_1^*/s)^2}{AR_c \cdot \sigma} \right]^{3/4} \quad (deg)$$

FIGURE 9.

SPANWISE POSITION OF MAXIMUM UNDERTURNING

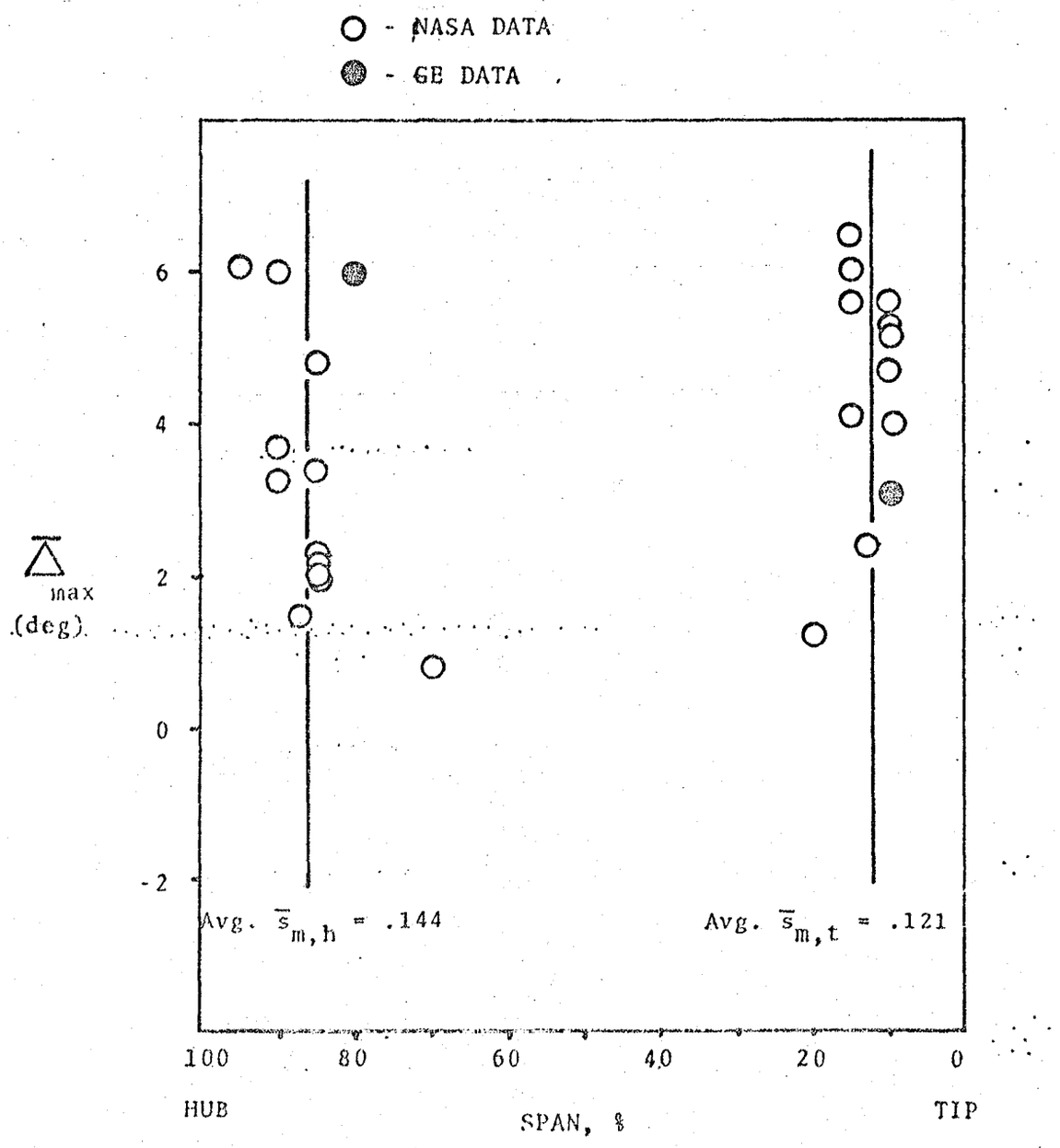

FIGURE 10. ILLUSTRATION OF REASONABLE REGION OF MAXIMUM TO MINIMUM EXTRAPOLATION FOR END-WALL VALUE OF DEVIATION DIFFERENCE

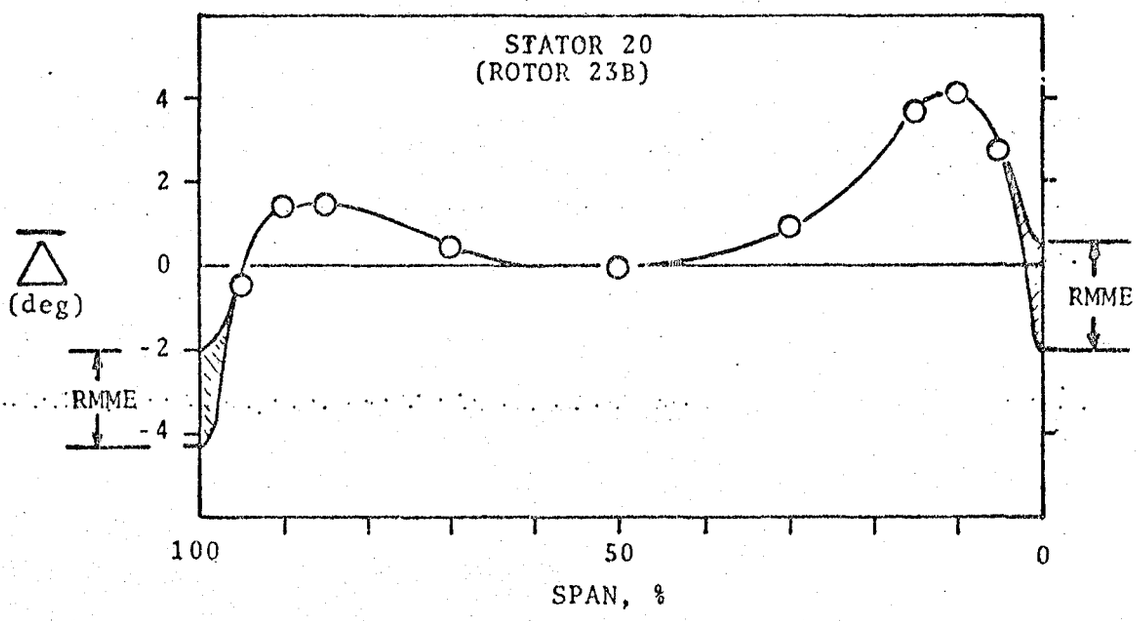

RMME - Region of Maximum to Minimum Extrapolation

FIGURE 11.

CORRELATION FOR DIFFERENCE IN
UNDERTURNING BETWEEN MAXIMUM
AND THE WALL

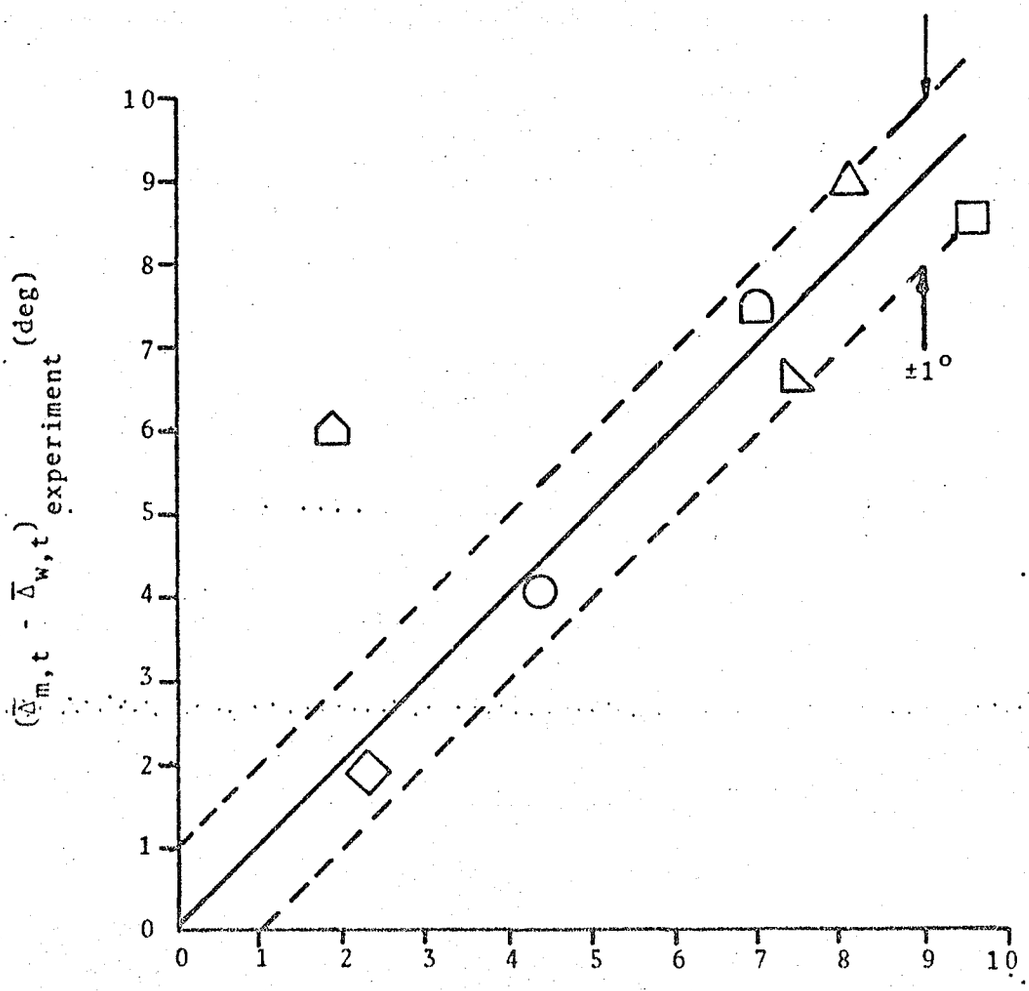

$$\bar{\Delta}_{max} - \bar{\Delta}_{w} = 5.7 \times 10^{5} \left[\frac{\phi(\delta^*/s)}{R_c \cdot \sigma}\right] \text{ (deg)}$$

FIGURE 12. COMPARISON OF SPANWISE DEVIATION MODEL WITH EXPERIMENT

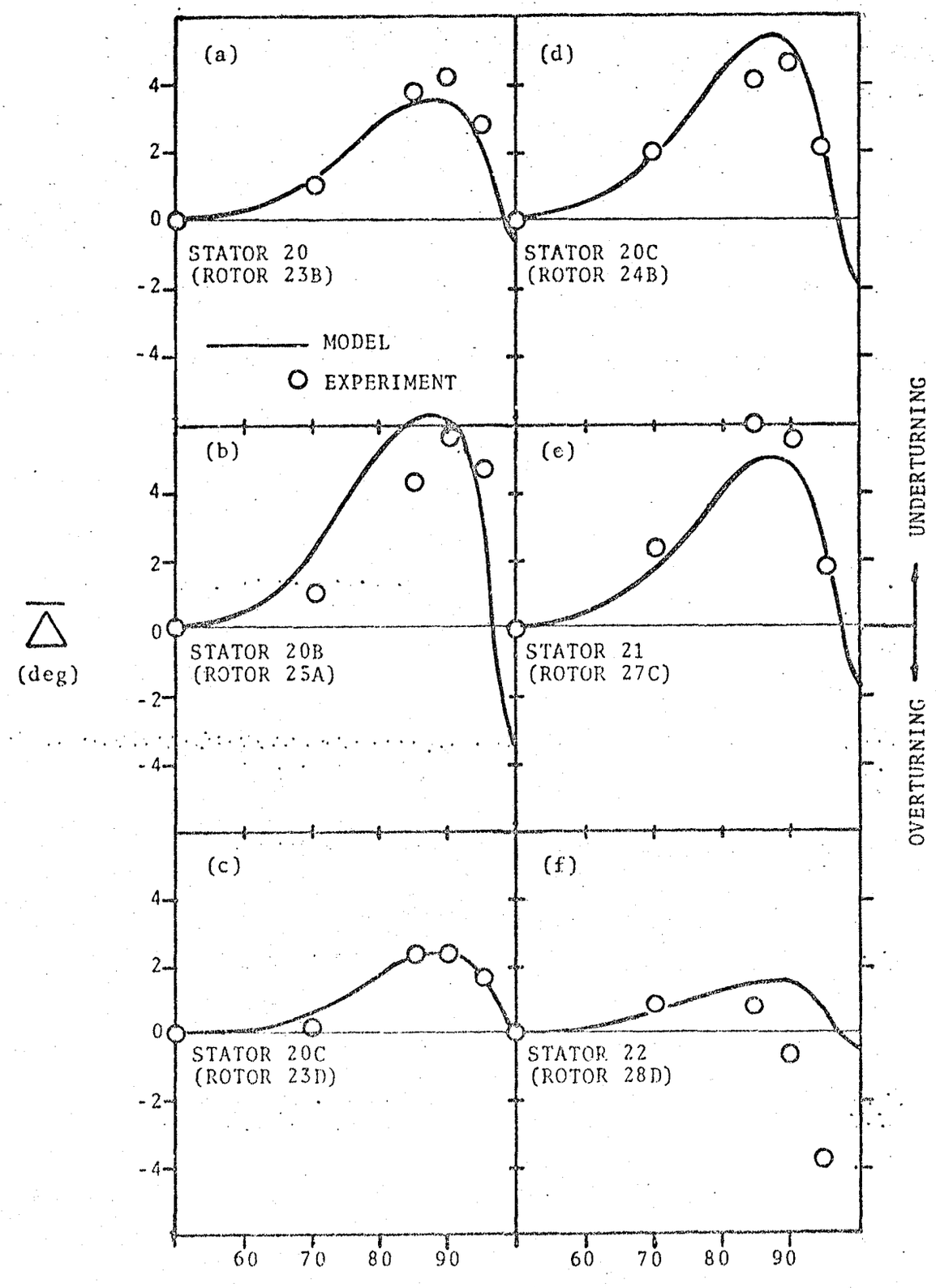

End of Document